RSC Advances

This is an *Accepted Manuscript*, which has been through the Royal Society of Chemistry peer review process and has been accepted for publication.

Accepted Manuscripts are published online shortly after acceptance, before technical editing, formatting and proof reading. Using this free service, authors can make their results available to the community, in citable form, before we publish the edited article. This *Accepted Manuscript* will be replaced by the edited, formatted and paginated article as soon as this is available.

You can find more information about *Accepted Manuscripts* in the Information for Authors.

Please note that technical editing may introduce minor changes to the text and/or graphics, which may alter content. The journal's standard Terms & Conditions and the Ethical guidelines still apply. In no event shall the Royal Society of Chemistry be held responsible for any errors or omissions in this *Accepted Manuscript* or any consequences arising from the use of any information it contains.

ROYAL SOCIETY OF CHEMISTRY

www.rsc.org/advances

Journal Name RSCPublishing

ARTICLE

Direct Growth of Sb_2Te_3 on Graphene by Atomic Layer Deposition

Cite this: DOI: 10.1039/x0xx00000x

Received 00th March 2015, Accepted 00th April 2015

DOI: 10.1039/x0xx00000x

www.rsc.org/

Li Zheng,[ab] Xinhong Cheng*[a], Duo Cao, [ab] Qian Wang,[ab] Zhongjian Wang, [a] Chao Xia, [ab] Lingyan Shen,[ab] Yuehui Yu[a] and Dashen Shen[c]

The direct growth of Sb_2Te_3 on graphene is achieved by atomic layer deposition (ALD) with pre-$(Me_3Si)_2Te$ treatment. The results of atomic force microscopy (AFM) indicate Volmer-Weber island growth is the dominant growth mode for ALD Sb_2Te_3 growth on graphene. High resolution transmission electron microscopy (HRTEM) analysis reveals perfect crystal structures of Sb_2Te_3 on graphene and no interface layer generation. The characterization of X-ray photoelectron spectroscopy (XPS) implies the impermeability of graphene can maintain Sb_2Te_3 intact and isolate the adverse effects of substrates. Our study provides a step forward to grow high quality of Sb_2Te_3 at low temperature and expand the potential applications of graphene in ALD techniques.

Introduction

The recent theoretical prediction and experimental realization of Sb_2Te_3 and Bi_2Te_3, have generated intense interest in a new state of quantum matter, known as a topological insulator (TI), from both materials science and condensed matter physics.[1-6] The TI material is insulating in bulk with a finite band gap but possesses a gapless surface state protected by time reversal symmetry (TRS).[1-3] The interplay between the topological order and symmetry breaking in a TI may leads to many proposals of novel quantum phenomena such as anomalous quantum Hall effect and Majorana fermions, and pave the way for superconductor and quantum computation applications.[4-6] Furthermore, Sb_2Te_3 and Bi_2Te_3 can act as thermoelectric materials and have potential applications in power generation and refrigeration systems.[7-12] The efficiency of thermoelectric materials is expressed by the dimensionless figure of merit (*ZT*), which is defined as $ZT = S^2\boldsymbol{\sigma}T/(\boldsymbol{\kappa}_l + \boldsymbol{\kappa}_e)$, where S is the Seebeck coefficient, $\boldsymbol{\sigma}$ is the electrical conductivity, T is the absolute temperature, and $\boldsymbol{\kappa}_l + \boldsymbol{\kappa}_e$ are the thermal conductivity. R. Venkatasubramanian et al. reported that Sb_2Te_3 and Bi_2Te_3 can be grown on GaAs by metal-organic chemical vapor deposition (MOCVD).[13] Molecular beam epitaxy (MBE) have also been demonstrated to grow Sb_2Te_3 and Bi_2Te_3 on graphene by Xue et. al.[6,14] Graphene has a similar layered structure to Sb_2Te_3/Bi_2Se_3 and is chemically inert due to the strong bonding of carbon atoms, which turns out to greatly suppress interface reaction leading to atomically sharp interface between Sb_2Te_3/Bi_2Se_3 and graphene.[15-18] However, high growth temperature during the MOCVD and MBE processes results in the issues of interlayer outdiffusion and thermal lattice mismatch, which in turn adversely affect the thermoelectric performance.[19] Therefore, a relatively low temperature growth technique should be explored for Sb_2Te_3 or Bi_2Te_3 deposition. Atomic layer deposition (ALD) has been proven to be an excellent technique to deposit thin films with atomic level precision and uniformity of large area. In addition, the growth temperature of ALD is rather low in comparison with other thin film deposition processes. Nevertheless, graphene surface is chemical insert and there are no dangling bonds on it. Dangling bonds are required for surface chemical reactions, which are the conventional ALD processes based on. Wang et al. have reported that without any pre-treatment, ALD of thin films gives no direct deposition on defect-free pristine graphene and dangling bonds existing only on the edges and defect sites of graphene, can react with ALD precursors to afford active thin film growth.[20] Functionalization of graphene via NO_2 or O_3 has also been performed to introduce defects into graphene and supply more dangling bonds on graphene for subsequent ALD processes.[21,22] However, high quality of graphene with excellent impermeability plays a key role in Sb_2Te_3 deposition and no defects in graphene are expected. If there are defects in graphene, the impermeability of graphene will be deteriorated, which may lead to oxidation of Sb_2Te_3 by the hydroxide radicals on the substrates and generation of an interface layer. Moreover, there are several dangling bonds at the defects of graphene, which can react with precursors and further decrease the quality of Sb_2Te_3. In this work, we utilized physically absorbed $(Me_3Si)_2Te$ on graphene to act as nucleation sites for ALD $(Me_3Si)_2Te$ growth and the ALD growth mechanism of Sb_2Te_3 on graphene was analyzed. No defects were introduced into graphene during the ALD processes and the impermeability of graphene could be well preserved. AFM was performed to investigate the surface morphology transformation of Sb_2Te_3 on different substrates. HRTEM was utilized to manifest the cross-section structure of Sb_2Te_3 on graphene and XPS was carried out to reveal the elemental constituents of Sb_2Te_3 grown on graphene by ALD.

Experimental section

RSC Advances Accepted Manuscript

This journal is © The Royal Society of Chemistry 2015

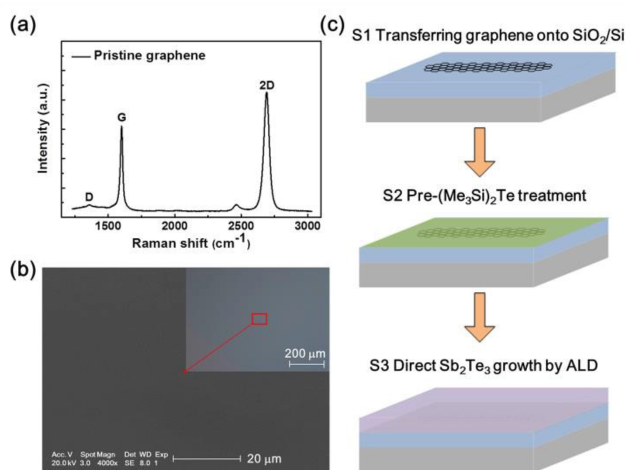

Fig. 1 (a) Raman spectroscopy of graphene. (b) The SEM micrograph of graphene on SiO_2/Si (Inset: the optical microscope of graphene on SiO_2/Si). (c) The flow chart of Sb_2Te_3 growth on graphene by ALD.

Graphene films were grown on a Cu foil (0.025 mm, 99.8%) in a low pressure CVD system. During the graphene growth process, the quartz tube was maintained at 1050℃ for 60 min under the flow of 50 sccm H_2 and 10 sccm CH_4. The as-grown graphene on Cu was spin-coated with poly-methyl methacrylate (PMMA) and baked at 180℃ for 3 min. $FeCl_3$ solution (0.1 M) was used to dissolve the Cu foil. Then, PMMA-graphene was rinsed in deionized water and transferred onto Si substrates covered by 300 nm thickness of SiO_2 (SiO_2/Si). Acetone was used to remove PMMA and graphene was annealed at 200℃ for 3 hours under the flow of 10 sccm Ar and 50 sccm H_2 to remove the photoresist residue before ALD processes. The H_2 shielding could admirably prevent graphene from being oxidized by O_2 existing at the interface between graphene and substrates. For comparison, other substrates such as Si, Si with native oxide and SiO_2/Si were also annealed under Ar and H_2 mixture gas. The graphene flakes were monolayers with few defects and no detectable photoresist residue confirmed by Raman spectroscopy analysis (Figure 1a) and scanning electron microscope (SEM)/optical microscope measurements (Figure 1b), respectively. All the graphene samples were grown and transferred at the same condition.

$SbCl_3$ and (trimethylsilyl)telluride [$(Me_3Si)_2Te$] were applied as precursors for Sb_2Te_3 growth in a commercial ALD reactor (BENEQ TFS 200-124) maintained at a low level of base pressure by a vacuum pump (Adixen). $SbCl_3$ was pre-heated to 70℃ while $(Me_3Si)_2Te$ was pre-heated to 45℃. Nitrogen gas (99.999% in purity) was used as a carrier gas at a flow rate of 10 sccm. The flow chart of ALD growth of Sb_2Te_3 on graphene was illustrated in Figure 1c. After graphene was transferred onto SiO_2/Si (Step 1), several cycles of $(Me_3Si)_2Te$ were firstly introduced into ALD chamber and absorbed on graphene by the van der Waals attraction to act as deposition sites (Step 2). The utilization of pre-$(Me_3Si)_2Te$ in preference to pre-$SbCl_3$ treatment to act as deposition sites was due that tellurium vacancies were inclined to generate during Sb_2Te_3 growth.[4,6] Then, $(Me_3Si)_2Te$ and $SbCl_3$ were introduced into ALD chamber for Sb_2Te_3 growth (Step 3). One ALD cycle was executed with the completion of following four steps: (1) a 1 s pulse of $(Me_3Si)_2Te$ in duration; (2) a 20 s purge of excess $(Me_3Si)_2Te$ and any byproducts; (3) a 1 s supply of $SbCl_3$; (4) a 20 s purge of excess $SbCl_3$ and any byproducts.

Results and discussion

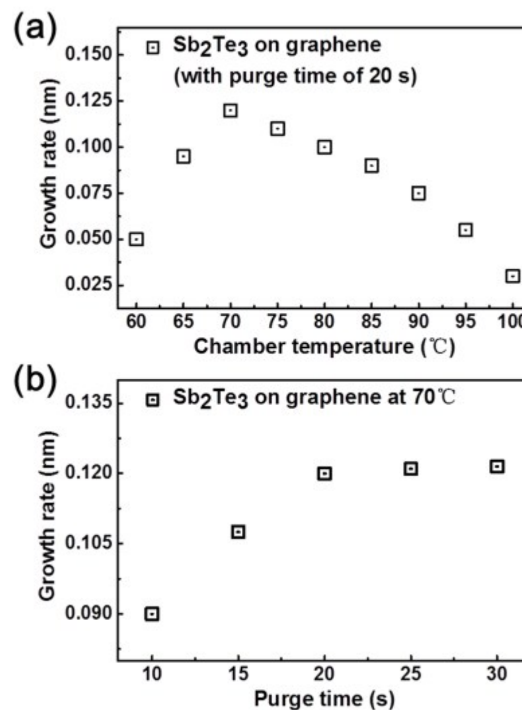

Fig. 2 (a) The relationship between growth rate of Sb_2Te_3 and ALD chamber temperatures. (b) The relationship between growth rate of Sb_2Te_3 and ALD purge time.

To experimentally establish the optical ALD temperature window for Sb_2Te_3 grown on graphene, systematic ALD experiments were conducted by varying the growth temperature from 60℃ to 100℃ with a temperature interval of 5℃. The normal growth rate of ALD is 0.08-0.15 nm/cycle. Based on this, the suited chamber temperatures for Sb_2Te_3 growth were 65-85℃, as shown in Figure 2a. The highest growth rate of Sb_2Te_3 was 0.12 nm/cycle at 70℃, which probably because the Sb-precursor ($SbCl_3$) reached to its saturated vapor pressure at 70℃. If the ALD chamber temperature was lower than 70℃, the growth rate would decrease due to unsaturated vapor pressure of $SbCl_3$ at low temperature; if the ALD chamber temperature was higher than 70℃, the enhanced desorption of $(Me_3Si)_2Te$ from graphene would lead to deficient nucleation sites for Sb_2Te_3 deposition, which also resulted in the decrease of growth rate. Therefore, the chosen chamber temperatures for Sb_2Te_3 growth was 70℃. As illustrated in Figure 2b, the extension of purge time benefitted for the increase of Sb_2Te_3 growth rate, which was possibly due to more nucleation sites and more adequate reaction between $(Me_3Si)_2Te$ and $SbCl_3$ at longer purge time. When the purge time was extended to 20 s, the growth rate of Sb_2Te_3 tended to be saturation and further increasing the purge time had few effects on the growth rate of Sb_2Te_3 on graphene.

RSC Advances Accepted Manuscript

 This journal is © The Royal Society of Chemistry 2015

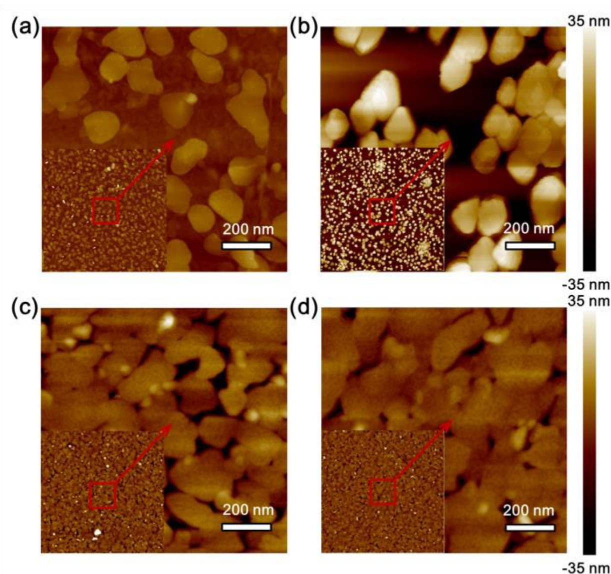

Fig. 3 AFM images of Sb_2Te_3 on graphene (a), Si (b), Si with native oxide (c) and Si covered with 300 nm thickness of SiO_2 (d).

The AFM micrograph of Sb_2Te_3 on graphene illustrated that Volmer-Weber island growth rather than monolayer-upon-monolayer growth was the dominant growth mode for ALD Sb_2Te_3 growth on graphene. The Volmer-Weber mechanism was characterized by island growth and heterogeneous nucleation as shown in Figure 3a. In the Volmer-Weber growth mechanism, interactions between atoms dominated over interactions of atoms with the surface, resulting in the formation of three dimensional atom clusters and islands. In the nucleation phase, the Sb_2Te_3 films did not wet well on graphene due to hydrophobicity of graphene and a lack of dangling bonds at the Te-terminated surfaces of Sb_2Te_3, which led to heterogeneous nucleation and island growth. In order to verify the cause, Sb_2Te_3 was also deposited on Si, Si with native oxide and SiO_2/Si at the same growth condition, respectively. The surface of Si was also hydrophobic and the morphology of Sb_2Te_3 on Si (shown in Figure 3b) was similar to Sb_2Te_3 on graphene. However, the height of Sb_2Te_3 islands on Si was not consistent, which was possibly due to lattice mismatch between Sb_2Te_3 and Si. The surface of Si with native oxide had several hydroxyl bonds, which could oxidize Te-terminated surfaces of Sb_2Te_3 and result in dangling bonds increase.[2,23] Therefore, the individual nucleated islands of Sb_2Te_3 on Si with native oxide tended to coalesce into a continuous layer (shown in Figure 3c). The surface of SiO_2/Si was hydrophilic and Sb_2Te_3 could well wet on SiO_2/Si. In addition, Te-terminated surfaces of Sb_2Te_3 could be further oxidized due to more hydroxyl bonds on SiO_2/Si surface, leading to a planar film of Sb_2Te_3 on SiO_2/Si (shown in Figure 3d). It is worth to mention that Te-terminated surfaces oxidation of Sb_2Te_3 will introduce impurities into Sb_2Te_3 and generate an interface layer, which both deteriorate the property of Sb_2Te_3. Therefore, it is prerequisite to avoid oxidation of Sb_2Te_3 during its growth process. The impermeability of graphene can efficiently isolate the hydroxide radicals on the substrates and avoid Te-terminated surfaces oxidized. To investigate the excellent effect of graphene on ALD Sb_2Te_3 growth, HRTEM and XPS were carried out to manifest the cross-section structure and elemental constituents of Sb_2Te_3 on graphene, respectively.

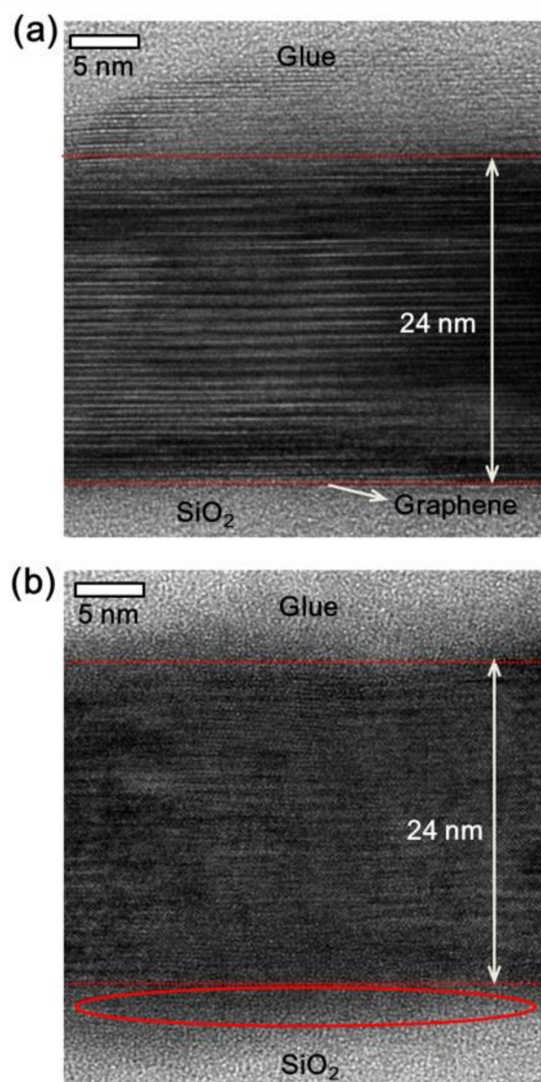

Fig. 4 Cross-section HRTEM images of Sb_2Te_3 on graphene (a) and SiO_2/Si (b).

HRTEM was implemented to reveal the cross-section structures of Sb_2Te_3 grown on graphene and SiO_2, respectively. Since Volmer-Weber island growth was the dominant growth mechanism, one fine structure of a large island was examined at high magnification. As shown in Figure 4a, Sb_2Te_3 showed perfect crystal structures with the lattice planes aligned parallel to graphene surface and the thickness of Sb_2Te_3 on graphene was 24 nm. In addition, no discernible interface layer was visible between Sb_2Te_3 and graphene. The thickness of Sb_2Te_3 on SiO_2 was also 24 nm (excluding the interfaces) as shown in Figure 4b. However, the crystal structures of Sb_2Te_3 on SiO_2 were anomalous and partial regions were blurry to detect. The interface layer between Sb_2Te_3 and SiO_2 was obvious with an amorphous morphology (labeled by a red elliptical ring in Figure 4b), implying hydroxide radicals on SiO_2 could react with Sb_2Te_3 and introduce impurity defects into Sb_2Te_3. Therefore, graphene was conducive to the maintenance of Sb_2Te_3 crystal structures, especially at the interfaces.

RSC Advances Accepted Manuscript

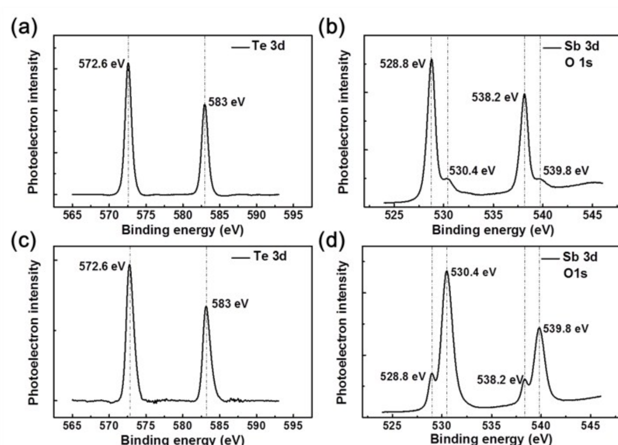

Fig. 5 XPS analysis of Sb_2Te_3 on different substrates: graphene (a) and SiO_2/Si (b).

In order to further demonstrate the advantageous effect of graphene on the property enhancement of Sb_2Te_3, the elemental constituents of ALD Sb_2Te_3 grown on graphene and SiO_2 were both characterized by XPS as shown in Figures 5a-d. All the XPS peaks were calibrated with the C 1s peak position at 284.8 eV. For both samples, Te 3d peaks could be fitted at 573.6 eV (Te $3d_{3/2}$) and 583 eV (Te $3d_{5/2}$) and Sb 3d peaks could be fitted at 528.8 eV (Sb $3d_{3/2}$) and 538.2 eV (Sb $3d_{5/2}$). In addition, the binding energy difference between Te $3d_{3/2}$ and Te $3d_{5/2}$ was 9.4 eV and the binding energy difference between Sb $3d_{3/2}$ and Sb $3d_{5/2}$ was 9.4 eV as well, in agreement with reported values of Sb_2Te_3.[24] As shown in Figure 5b, the O 1s peaks locating at 530.4eV and 539.8 eV of Sb_2Te_3 on graphene were not obvious, indicating graphene could efficiently avoid oxidation of Sb_2Te_3 by hydroxyl bonds on SiO_2. However, the O 1s peaks of Sb_2Te_3 on SiO_2 were very strong (shown in Figure 5d), implying that Sb_2Te_3 was seriously oxidized. Therefore, graphene also contributed to maintaining Sb_2Te_3 intact and isolated the adverse effects of substrates.

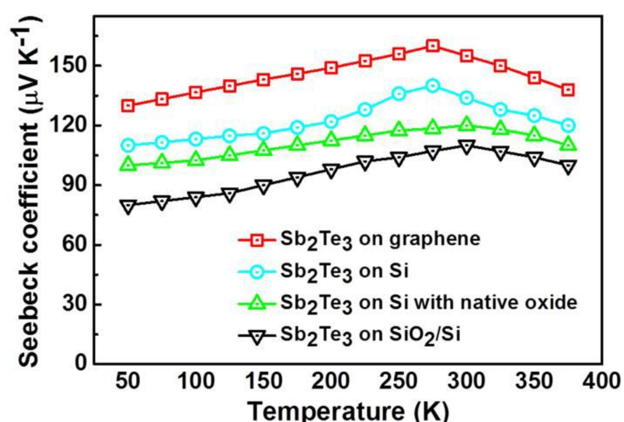

Fig. 6 Temperature dependent Seebeck coefficients of Sb_2Te_3 on different substrates: graphene (red squares), Si (blue circles), Si with native oxide (green triangles) and SiO_2/Si (inverted triangle triangles).

Figure 6 shows the Seebeck coefficients of Sb_2Te_3 on graphene, Si, Si with native oxide and SiO_2/Si as a function of temperatures, respectively. As for Sb_2Te_3 on graphene, the Seebeck coefficient increased up to a maximum of 158 $\mu V\ K^{-1}$ at 275 K, which was comparable to the values reported of Sb_2Te_3 in the literature.[25-26] Compared to Sb_2Te_3 on graphene, the Seebeck coefficient of Sb_2Te_3 on Si was observably decreased, which was due to deteriorated quality of Sb_2Te_3 resulted from lattice mismatch between Sb_2Te_3 and Si. The Seebeck coefficient of Sb_2Te_3 on Si with native oxide was further decreased. Hydroxyl bonds existing on the surface of Si with native oxide could oxidize Te-terminated surfaces of Sb_2Te_3 and introduce oxide impurity in Sb_2Te_3, leading to property deterioration of Sb_2Te_3. For the four control samples, the Seebeck coefficient of Sb_2Te_3 on SiO_2/Si was the lowest. Sb_2Te_3 could well wet on SiO_2/Si due to abundant hydroxyl bonds on its surface. Te-terminated surfaces of Sb_2Te_3 would be further oxidized, introducing more impurities into Sb_2Te_3 and generating an obvious interface layer (shown in Figure 4b), which both deteriorated the property of Sb_2Te_3. Therefore, graphene could effectively avoid the adverse effect from the substrates and maintain the thermoelectric performance of Sb_2Te_3.

Conclusions

In summary, Sb_2Te_3 can be directly deposited on graphene by ALD with assistance of pre-$(Me_3Si)_2Te$ treatment. Volmer-Weber island growth rather than monolayer-upon-monolayer growth is the dominant growth mode for ALD Sb_2Te_3 growth on graphene. Graphene can efficiently avoid oxidation of Sb_2Te_3 by hydroxide radicals on the substrates, eliminate the generation of an interface layer and maintain the crystal structures of Sb_2Te_3. This technique represents a solid step forward in preparing low-temperature-grown thermoelectric materials and expanding the potential applications of graphene in ALD techniques.

Acknowledgements

This work is funded by the National Natural Science Foundation of China (Grant No. 11175229).We would like to thank Pro. Zengfeng Di, Dr. Zhiqiang Mu and Dr. Haoran Zhang for their generous help.

Notes and references

[a] *State Key Laboratory of Functional Materials for Informatics, Institute of Microsystem and Information Technology, Chinese Academy of Sciences, Shanghai 200050, China. E-mail: xh_cheng@mail.sim.ac.cn.*
[b] *University of Chinese Academy of Sciences, Beijing 100049, China.*
[c] *University of Alabama in Huntsville, Huntsville, Alabama 35899, America.*

1 J. E. Moore, *Nature*, 2010, **464**, 194-198.
2 Y. L.Chen, J. G. Analytis, J. Chu, Z. K. Liu, S. Mo, X. Qi, H. J. Zhang, D. H. Lu, X. Dai, Z. Fang, S. C. Zhang, I. R. Fisher, Z. Hussain and Z. Shen, *Science*, 2009, **325**, 178-181.
3 M. Wang, C. Liu, J. Xu, F. Yang, L. Miao, M. Yao, C. L. Gao, C. Shen, X. Ma, X. Chen, Z.Xu, Y. Liu, S. Zhang, D. Qian, J. Jia and Q. Xue, *Science*, 2012, **336**, 52-55.
4 Xi Chen, Xu Ma, K. He, J. Jia and Q. Xue, *Adv. Mater.*, 2011, **23**, 1162–1165.
5 L. Fu, C. L. Kane and E. J. Mele, *Phys. Rev. Lett.*, 2007, **98**, 106803.

RSC Advances Accepted Manuscript

This journal is © The Royal Society of Chemistry 2015

6 Y. Jiang, Y. Sun, M. Chen, Y. Wang, Z. Li, C. Song, K. He, L. Wang, X. Chen, Q. Xue, X. Ma and S. B. Zhang, *Phys. Rev. Lett.*, 2012, **108**, 066809.

7 V. Pore, T. Hatanpää, M. Ritala and M. Leskelä, *J. Am. Chem. Soc.*, 2009, **131**, 3478–3480.

8 K. Knapas, T. Hatanpä, M. Ritala and M. Leskelä, *Chem. Mater.*, 2010, **22**, 1386–1391.

9 S. Urazhdin, D. Bilc, S. D. Mahanti, S. H. Tessmer, T. Kyratsi and M. G. Kanatzidis, *Phys. Rev. B*, 2004, **69**, 085313.

10 Z. Zhang, S. Song, Z. Song, Y. Cheng, Y. Gu and B. Chen, *Appl. Phys. Lett.*, 2013, **102**, 252106.

11 Y. C. Dou, X. Y. Qin, D. Li, L. L. Li, T. H. Zou and Q. Q.Wang, *J. Appl. Phys.*, 2013, **114**, 044906.

12 S. Zastrow, J. Gooth, T. Boehnert, S. Heiderich, W. Toellner, S. Heimann, S. Schulz and K. Nielsch, *Semicond. Sci. Technol.*, 2013, **28**, 035010.

13 R. Venkatasubramanian, T. Colpitts, B. O'Quinn, S. Liu, N. El-Masry and M. Lamvik, *Appl. Phys. Lett.*, 1999, **75**, 1104.

14 C. Song, Y. Wang, Y. Jiang, Y. Zhang, C. Chang, L. Wang, K. He, X. Chen, J. Jia, Y. Wang, Z. Fang, X. Dai, Xi. Xie, X. Qi, S. Zhang, Q. Xue and X. Ma, *Appl. Phys. Lett.*, 2010, **97**, 143118.

15 K. S. Novoselov, A. K. Geim, S. V. Morozov, D. Jiang, Y. Zhang, S. V. Dubonos, I. V. Grigorieva and A. A. Firsov, *Science*, 2004, **306**, 666-669.

16 L. Zheng, X. Cheng, D. Cao, G. Wang, Z. Wang, D. Xu, C. Xia, L. Shen, Y, Yu and D. Shen, *ACS Appl. Mater. Interfaces*, 2014, **6**, 7014−7019.

17 A. Ambrosetti and P. L. Silvestrelli, *J. Phys. Chem. C*, 2011, **115**, 3695–3702.

18 L. Zheng, X. Cheng, D. Cao, D. Zhang, Z. Wang, D. Xu, C. Xia, L. Shen and Y, Yu, *RSC Adv.*, 2014, **4**, 44296-44301.

19 D. Nminibapiel, K. Zhang, M. Tangirala, H. Baumgart, V. S. K. Chakravadhanula, C. Kübel and V. Kocherginf, *ECS J. of Solid State SC*, 2014, **3**, 95-100.

20 X. Wang, S. M. Tabakman and H. Dai, *J. Am. Chem. Soc.*, 2008, **130**, 8152–8153.

21 J. R Williams, L. DiCarlo and C. M. Marcus, *Science*, 2007, **317**, 638–641.

22 S. Jandhyala, G. Mordi, B. Lee, G. Lee, C. Floresca, P. -R. Cha, J. Ahn, R. M. Wallace, Y. J. Chabal, M. J. Kim, L. Colombo, K. Cho and J. Kim, *ACS Nano*, 2012, **6**, 2722–2730.

23 K. Knapas, T. Hatanpää, M. Ritala and M. Leskelä, *Chem. Mater.*, 2010, **22**, 1386–1391.

24 G. Hao, X. Qi, Y. Fan, L. Xue, X. Peng, X. Wei and J. Zhong. *Appl. Phys. Lett.*, 2013, **102**, 013105.

25 M. Winkler, X. Liu, J. D. Konig, S. Buller, U. Schürmann, L. Kienle, W. Bensch and H. Bottner. *J. Mater. Chem.*, 2012, **22,** 11323.

26 S. Zastrow, J. Gooth, T. Boehnert, S. Heiderich, W. Toellner, S. Heimann, S. Schulz and K. Nielsch. *Semicond. Sci. Technol.*, 2013, **28**, 035010.

RSC Advances Accepted Manuscript